Estimation of river discharge, propagation speed, and hydraulic geometry from space: Lena River, Siberia

Laurence C. Smith[1,2] and Tamlin M. Pavelsky[1]

Received 23 April 2007; revised 19 October 2007; accepted 19 December 2007; published 27 March 2008.

[1] Moderate Resolution Imaging Spectroradiometer (MODIS)–derived measurements of Lena River effective width (W_e) display a high predictive capacity ($r^2 = 0.81$, mean absolute error < 25%) to forecast downstream discharge conditions at Kusur station, some 8 d and ~700 km later. Satellite-derived mean flow propagation speed (88 km d^{-1} or 1.01 m s^{-1}) compares well with that estimated from ground data (84 km d^{-1} or 0.97 m s^{-1}). Scaling analysis of a ~300 km heavily braided study reach suggests that at length scales > 60–90 km (~2–3 time valley width), satellite-derived $W_e - Q$ rating curves and hydraulic geometry (*b* exponents) converge upon stable values ($b = 0.48$), indicating transferability of the discharge retrieval method between different locations. Put another way, at length scales exceeding ~60–90 km all subreaches display similar behavior everywhere. At finer reach length scales (e.g., 0.25–1 km), longitudinal extraction of *b* exponents represents the first continuous mapping of a classical hydraulic geometry parameter from space. While at least one gauging station is required for calibration, results suggest that multitemporal satellite data can powerfully enhance our understanding of water discharge and flow conveyance in remote river systems.

Citation: Smith, L. C., and T. M. Pavelsky (2008), Estimation of river discharge, propagation speed, and hydraulic geometry from space: Lena River, Siberia, *Water Resour. Res.*, *44*, W03427, doi:10.1029/2007WR006133.

1. Introduction

[2] Measurements of river discharge are required for flood hazard management, water resource planning, climate and ecology studies, and compliance with transboundary water agreements. Knowledge of river propagation speed, the time for flows to pass downstream, is critical for flood forecasting, reservoir operations, and watershed modeling. However, gauging station records are generally sparse outside of North America and Europe, even though the most ominous projections of future water supply shortages lie outside of these regions [*Vörösmarty et al.*, 2000]. Even where good monitoring networks exist, hydrologic conditions between stations must be interpolated or modeled, often over long distances. In the developing world, streamflow data are seldom available for economic, political, and proprietary reasons. Data are also sparse in the high latitudes (and declining) [*Shiklomanov et al.*, 2002], where low population, ice jams, and predominance of braided gravel bed rivers limit river gauging. This impedes our understanding of Arctic climate warming, which is believed to exert strong impacts on terrestrial hydrology [*Wu et al.*, 2005; *Stocker and Raible*, 2005].

[3] For these and other reasons, the last decade has seen a rising interest in the potential for satellites to remotely estimate streamflow [*Alsdorf and Lettenmaier*, 2003; *Brakenridge et al.*, 2005; *Alsdorf et al.*, 2007]. In general, a remote-sensing approach is best suited for large, remote rivers [*Hudson and Colditz*, 2003; *Roux and Dartus*, 2006]. Most space-based efforts have sought to measure discharge at specific locations along a river course, much like ground-based gauging stations. In rarer cases, the broad synoptic view afforded from space has been exploited to obtain fundamentally new hydrologic observations that could not realistically be achieved on the ground [e.g., *Smith and Alsdorf*, 1998; *Alsdorf et al.*, 2000; *Smith*, 2002; *Richey et al.*, 2002; *Birkett et al.*, 2002; *Alsdorf*, 2003; *Frappart et al.*, 2005; *Smith et al.*, 2005; *Andreadis et al.*, 2007; *Grippa et al.*, 2007]. Such promising results have prompted calls to the hydrologic community to move beyond traditional point-based gauging methods to new remote sensing measurements of the spatial variability inherent to surface water systems [*Alsdorf and Lettenmaier*, 2003; *Alsdorf et al.*, 2007].

[4] Whether ground or space based, a key limitation of many discharge estimation methods is their dependence upon empirical rating curves that relate occasional measurements of true river discharge (water flux, m^3/s or ft^3/s, taken in situ) to another variable (water level, inundation area) that can be monitored more easily. Because the rating curves are site specific, they cannot be applied elsewhere along the same river or to other rivers of similar form [*Bjerklie et al.*, 2003]. This site-specificity greatly increases the cost of ground-based river gauging and is a prime obstacle to a global capability to track river discharge from space.

[1]Department of Geography, University of California, Los Angeles, California, USA.
[2]Department of Earth and Space Sciences, University of California, Los Angeles, California, USA.

0043-1397/08/2007WR006133$09.00

[5] A further limitation of most satellite methods is low temporal sampling rate, typically weeks to months for high-resolution (~10–30 m) visible/near-infrared sensors [*Smith*, 1997]. However, unlike permanent gauging stations satellites observe river conditions with dense spatial sampling over large areas; and collect data globally including inaccessible, impoverished, or politically unstable regions. These benefits offer high scientific and societal value and are a prime motivator for developing a new, space-based approach to river measurement.

[6] Following a brief review of traditional versus remotely sensed discharge estimation methods, we examine to what extent the latter can be used to assess flow conditions far from existing gauging stations, i.e., in an upstream or "forecasting" mode. We also assess whether useful discharge estimates can be obtained using satellite data that have moderately poor spatial resolution (250 m) but high temporal sampling (~daily). Finally, we examine hydraulic geometry scaling properties to explore if at sufficiently large length scales, a stable (i.e., not site-specific) satellite-based rating curve emerges that may be reasonably applied elsewhere along the river course. These objectives are carried out for a remote, ~300 km braided reach of the Lena River, Siberia using downstream ground measurements of discharge and 5 years of NASA Moderate Resolution Imaging Spectroradiometer (MODIS) visible/near-infrared satellite data from 2001 to 2005.

2. Traditional Versus Remote Sensing Estimates of River Discharge: A Review

[7] The traditional framework for measurement of river discharge is the channel cross section, with total instantaneous discharge Q (water flux through the cross section, m^3/s or ft^3/s) equal to the product of mean cross-sectional flow width w, depth d, and velocity v ($Q = wdv$) as averaged from numerous in situ measurements taken across the stream. Mean w, d, and v all increase as a function of discharge, but the rate of increase for each varies with channel form giving rise to the so-called "at-a-station hydraulic geometry" of *Leopold and Maddock* [1953]. Under the hydraulic geometry framework, width, depth and velocity each possess distinct power law relationships with Q ($w = aQ^b$, $d = cQ^f$, $v = kQ^m$, with a, b, c, f, k, m empirically derived coefficients and $b + f + m$ and $a \times c \times k = 1$). The assumption that w, d, and v possess independent relationships with Q, while questionable [*Ferguson and Ashworth*, 1991], allows river discharge to be computed from any one of them if the corresponding coefficients are known. For the vast majority of ground-based gauging installations the variable of choice is flow depth d, recorded continuously as water level fluctuations in a stilling well vented to the stream. Occasional in situ measurements of Q are obtained to derive c and f, so that the continuously recorded measurements of d can be used compute Q. For best results a stable, single-channel cross section is required, preferably deep, narrow and in bedrock so that changes in discharge are accommodated largely by adjustments in flow depth. The exponent b (often called the "width exponent") is also widely used in fluvial geomorphology as a diagnostic measure of river behavior and form, e.g., high b exponents are characteristic of shallow, gravel bed rivers that accommodate discharge increases through channel widening, whereas low b exponents are typical of entrenched channels with cohesive banks. This traditional framework for measuring river discharge and hydraulic geometry is operational around the world and has remained largely unchanged since the 1800s and 1950s, respectively.

[8] Satellite remote sensing of river discharge is a much newer approach, with nearly all work done since the mid-1990s. The methods used have different variants, but a common approach is to simply correlate remotely sensed water levels (from altimetry) or inundation areas (from imaging) acquired at or near a gauging station with the simultaneous ground data [*Usachev*, 1983; *Smith et al.*, 1995, 1996; *Al-Khudhairy et al.*, 2002; *Townsend and Foster*, 2002; *Kouraev et al.*, 2004; *Xu et al.*, 2004; *Zhang et al.,* 2004; *Coe and Birkett*, 2004; *Brakenridge et al.*, 2005, 2007; *Temimi et al.*, 2005; *Ashmore and Sauks*, 2006; *Calmant and Seyler*, 2006; *Papa et al.*, 2007]. This is conceptually similar to the traditional method described above, except that a satellite-derived rather than ground-derived measurement is used, and (in the case of imaging systems) flow area or width, rather than depth, is the variable of choice. Another approach is to merge the satellite data with topographic information [*Brakenridge et al.*, 1994, 1998; *Sanyal and Lu*, 2004; *Bjerklie et al.,* 2005; *Matgen et al.*, 2007], output from hydraulic models [*Horritt and Bates*, 2002; *Bates et al.*, 2006; *Overton*, 2005; *Roux and Dartus*, 2006; *Leon et al.*, 2006; *Schumann et al.*, 2007], or informed estimates of channel depth and frictional resistance [*Lefavour and Alsdorf*, 2005]. A substantially different approach is to forgo discharge (flux) retrievals altogether, in favor of directly measuring three-dimensional water volume change over some defined area [*Alsdorf et al.*, 2001; *Alsdorf*, 2003; *Frappart et al.*, 2005, 2006].

[9] Strictly speaking, all remote sensing discharge methods are dimensionally incompatible with the traditional cross-section framework. In planform, w and d measured at a field cross section possess dimensions of length, whereas even the finest-resolution satellite sensors sample a two-dimensional area on the ground. An updating of hydraulic geometry theory to incorporate a two-dimensional river surface area variable a, (e.g., $a = gQ^h$) has yet to be formally articulated. Nonetheless, for the purpose of river discharge estimation the remote sensing community has largely treated its two-dimensional measurements as equivalent to the one-dimensional w, d, v of classical at-a-station hydraulic geometry. In the case of water level variations sampled by profiling altimeters, or flow widths extracted from image transects, the area effect is simply ignored. For discharge retrievals based on inundation area, the dimensional problem is often resolved by defining some river reach. Flow inundation areas measured within the reach are then divided by the reach length to yield one-dimensional units, dubbed "effective width" (W_e) [*Smith et al.*, 1995, 1996; *Ashmore and Sauks*, 2006]. Although W_e has the familiar units of width (m) it is derived from inundation area and should be thought of as a "reach-averaged" width rather than cross-sectional width [*Ashmore and Sauks*, 2006]. For discharge estimation, remotely sensed W_e values are then substituted for w in the hydraulic geometry formulation ($W_e = aQ^b$) and the equation inverted to compute Q. Like permanent gauging stations, an empirical rating curve must be constructed and the coefficients a and b calibrated

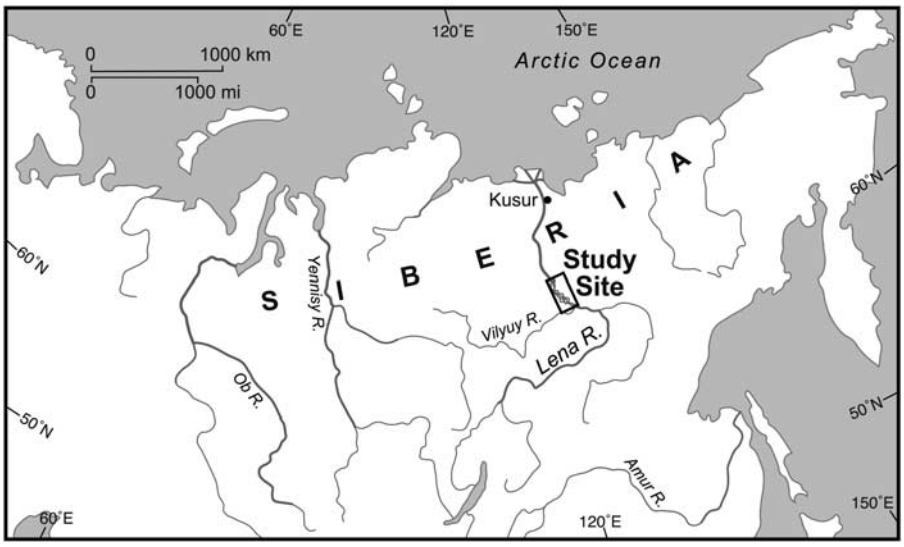

Figure 1. Location map of Lena River, our study site, and the permanent State Hydrologic Institute gauging station at Kusur.

using independent ground-based measurements of Q. Like traditional $d - Q$ rating curves, low variance in the $W_e - Q$ rating curve yields higher-quality discharge estimates.

3. Data and Study Region

[10] The Lena River is the world's eighth largest in terms of total annual flow volume (527 km^3/a) despite being frozen for 8 months of the year (October–May) [*Shiklomanov et al.*, 2006]. Since 1934, the Russian State Hydrologic Institute (SHI) has maintained a permanent gauging station at Kusur, about ~200 km upstream of the Lena's confluence with the Arctic Ocean and ~700 km downstream of the area examined in this paper (Figure 1). The drainage area upstream of Kusur station is $\sim 2.43 \times 10^6$ km^2 [*Shiklomanov et al.*, 2006], with minimum flows around ~2,000–5,000 m^3/s in winter (under ice) peaking rapidly to ~80,000–120,000 m^3/s during the annual spring flood. Mean absolute errors in corrected daily discharges from Kusur station average 17–28% from October to May (ice affected) and ~6% from June to September (ice free) [*Shiklomanov et al.*, 2006]. At the time of writing, corrected SHI daily discharge data are available only through 2001. Thereafter, only uncorrected "provisional" data are available from ArcticRIMS at the University of New Hampshire (http://rims.unh.edu/). The difference between corrected and provisional data also averages around 6% but varies (A. I. Shiklomanov, personal communication, 2007).

[11] At Kusur station the Lena River is a single-channel system. However, ~700 km upstream it is heavily braided, with numerous intertwining channels separated by tree-covered islands (Figures 1 and 2). In contrast to previous studies of proglacial, gravel bed braided rivers that shift constantly in response to varying discharge and sediment supply [*Smith et al.*, 1995, 1996], channel migration and new bar formation occur relatively slowly in the Lena, i.e., at decadal rather than subannual timescales [*Chalov*, 2001]. A remote, heavily braided, 316 km river reach in this area is the focus of this study (Figures 1 and 2).

[12] We obtained all cloud-free MODIS scenes acquired over the study site between 1 June and 30 September (open water season) in the years 2001, 2002, 2003, 2004, and 2005. Spring breakup periods were specifically excluded from consideration owing to floating ice debris and common ice jam floods that are clearly evident in MODIS images of the Lena [*Pavelsky and Smith*, 2004; *Brakenridge et al.*, 2007]. Band 2 data (near infrared, 0.841–0.876 m) were georeferenced and reprojected to 250 m spatial resolution using the MODIS Swath Reprojection Tool (http://edcdaac.usgs.gov/landdaac/tools/mrtswath/). Each scene was then thresholded to classify water from nonwater pixels. Off-nadir images were avoided to reduce the MODIS "bow tie" effect. To mitigate the effects of temporally varying sun angle, sensor angle, and atmospheric conditions on surface reflectance, the threshold was recomputed for each scene as the midpoint between the mean reflectance of 20 stable water pixels and 20 stable nonwater pixels, respectively. This produced a binary water map for each scene that closely matched a visual assessment of water extent.

[13] For each binary map, water inundation areas were extracted for a spectrum of reach length scales using RivWidth, a new software tool that automates the extraction of mean river widths from binary images of water extent [*Pavelsky and Smith*, 2008]. The output of RivWidth is nearly identical to W_e but is computationally faster and calculated in a slightly different manner. Rather than dividing inundated area by reach length, RivWidth derives a centerline for the study reach then computes the total width of all channels across a series of transects orthogonal to this centerline. The individual transect widths are then averaged over a user-defined length scale to provide a reach-averaged width. Because this value is nearly equivalent to W_e as calculated in previous studies we refer to it as such throughout the remainder of this paper. Derived values of W_e were then regressed against downstream ground observations of Q across the spectrum of reach scales, yielding

Table 1. Dates of MODIS Image Capture Over the Study Area, Derived Effective Widths, and Corresponding Predictions for Downstream Discharge 8 d Later[a]

	Study Reach	Kusur Station			
MODIS Date	W_e, m	Q_{t+8}, m^3/s	Q_p, m^3/s	$Q_p - Q_{t+8}$, m^3/s	$Q_p - Q_{t+8}$, %
10 Jun 2001	8577	60800	63115	2315	4
15 Jun 2001	7730	54900	53004	−1896	−3
10 Jul 2001	5216	24400	27372	2972	12
10 Jul 2001	4906	24400	24698	298	1
11 Jul 2001	5316	24200	28259	4059	17
17 Jul 2001	4376	20200	20377	177	1
22 Jul 2001	4363	18800	20281	1481	8
15 Aug 2001	4537	28300	21655	−6645	−23
15 Aug 2001	5190	28300	27141	−1159	−4
21 Aug 2001	5126	23400	26588	3188	14
23 Aug 2001	4779	20900	23628	2728	13
25 Aug 2001	4719	19700	23133	3433	17
29 Aug 2001	4156	18900	18690	−210	−1
30 Aug 2001	4519	18700	21513	2813	15
3 Sep 2001	3435	19100	13567	−5533	−29
7 Sep 2001	3608	18300	14740	−3560	−19
7 Sep 2001	4020	18300	17670	−630	−3
11 Jun 2002	8722	68700	64924	−3776	−5
14 Jun 2002	8624	61700	63707	2007	3
15 Jun 2002	8039	59300	56610	−2690	−5
28 Jun 2002	5948	39900	34133	−5767	−14
30 Jun 2002	7556	39200	51019	11819	30
20 Jul 2002	6608	34200	40729	6529	19
20 Jul 2002	6206	34200	36650	2450	7
14 Jun 2003	8790	68200	65772	−2428	−4
27 Jun 2003	7580	39200	51292	12092	31
9 Jul 2003	6961	36600	44450	7850	21
18 Jul 2003	6727	37950	41965	4015	11
21 Jul 2003	6959	34300	44432	10132	30
21 Jul 2003	6580	34300	40437	6137	18
16 Aug 2003	5872	20800	33402	12602	61
16 Aug 2003	5794	20800	32662	11862	57
17 Aug 2003	5902	20400	33687	13287	65
17 Aug 2003	5520	20400	30108	9708	48
17 Aug 2003	5864	20400	33327	12927	63
19 Aug 2003	5785	19900	32574	12674	64
31 Aug 2003	5838	22900	33077	10177	44
2 Sep 2003	5279	25400	27928	2528	10
3 Sep 2003	5569	24800	30555	5755	23
3 Sep 2003	5379	24800	28826	4026	16
4 Sep 2003	5267	24400	27820	3420	14
7 Jun 2004	8906	74800	67238	−7562	−10
9 Jun 2004	8691	67600	64539	−3061	−5
10 Jun 2004	8643	65900	63942	−1958	−3
6 Jul 2004	8227	51000	58848	7848	15
7 Jul 2004	8047	48600	56706	8106	17
12 Jul 2004	7607	36900	51591	14691	40
18 Jul 2004	8227	30300	58848	28548	94
20 Jul 2004	6677	26900	41442	14542	54
8 Aug 2004	6900	36000	43799	7799	22
16 Aug 2004	6895	31100	43744	12644	41
28 Aug 2004	6312	26700	37709	11009	41
2 Sep 2004	5889	20700	33561	12861	62
3 Sep 2004	5580	20100	30661	10561	53
19 Sep 2004	5030	24000	25752	1752	7
2 Jun 2005	7950	68700	55566	−13134	−19
9 Jun 2005	7925	49900	55267	5367	11
10 Jun 2005	7761	49000	53357	4357	9
19 Jun 2005	7481	52600	50165	−2435	−5
1 Jul 2005	7018	36900	45067	8167	22
7 Jul 2005	6897	39500	43769	4269	11
7 Sep 2005	6670	31600	41368	9768	31
7 Sep 2005	6264	31600	37229	5629	18
7 Sep 2005	6368	31600	38278	6678	21
7 Sep 2005	6639	31600	41051	9451	30

anywhere from one to 1264 rating curves and b exponents for the study site.

4. Results

[14] For the 5 year period 2001–2005, 65 cloud-free MODIS images were collected over the study area during the June–September open water period (Table 1). On nine occasions at least two cloud-free images were acquired on the same day (10 July 2001, 15 August 2001, 7 September 2001, 20 July 2002, 21 July 2003, 16 and 17 August 2003, 3 September 2003, and 7 September 2005; Table 1). Image processing of these data as described yields a time series of 65 measurements of W_e when averaged over the entire study reach, or many more measurements of W_e if the reach is subdivided further. Section 4.1 correlates overall W_e with daily discharges at Kusur station, ~700 km downstream, to assess discharge forecasting potential and average flow propagation speed. Section 4.2 explores spatial scaling of $W_e - Q$ rating curves and b exponents within the study reach, with implications for rating curve transferability and hydraulic geometry.

4.1. Forecasting of Downstream River Discharge From Upstream W_e

[15] A direct correlation between remotely sensed, reach-averaged Lena River effective widths (W_e) and same-day daily discharges at Kusur station (Q) reveals a power law relationship between the two variables ($r^2 = 0.71$, Figure 3a). Similar to *Ashmore and Sauks* [2006], we retain the power function because of its traditional use in hydrology. Although our application to an extremely large, tree-stabilized braided river is new, the result is otherwise consistent with previous findings of a power law or linear relationship between flow area and discharge [*Smith et al.*, 1995, 1996; *Townsend and Foster*, 2002; *Ashmore and Sauks*, 2006]. However, unlike earlier studies, the gauging station is located far downstream (~700 km) from the river reach used to sample W_e. At this distance, it is implausible that the measured W_e variations capture simultaneous discharge at the gauging station. Instead, they capture upstream discharges that will arrive at the station some time later. Lag analysis reveals a maximum goodness of fit between W_e and Q when a delay t of 8 d is introduced between the two time series (i.e., $r^2 = 0.77$ at $t = 8$, Figures 3b and 3c). The value t obtained in this manner represents a space-based measurement of average flow propagation speed [*Temimi et al.*, 2005; *Brakenridge et al.*, 2007], a key parameter in flow routing schemes. Dividing t by the travel distance to Kusur station yields an average propagation speed of 88 km d^{-1} (1.01 m s^{-1}). This remotely sensed estimate is remarkably similar to the value of 84 km d^{-1} (0.97 m s^{-1}) using discharge data from Tabaga station (1220 km upstream) obtained for 2000 and 2001 (A. I. Shiklomanov, personal communication, 2007).

Notes to Table 1:

[a] W_e is effective width, and Q_p is corresponding predictions for downstream discharge 8 d later. Also shown are the actual downstream discharges observed 8 d later at Kusur station (Q_{t+8}) and the differences between predicted and observed values ($Q_p - Q_{t+8}$).

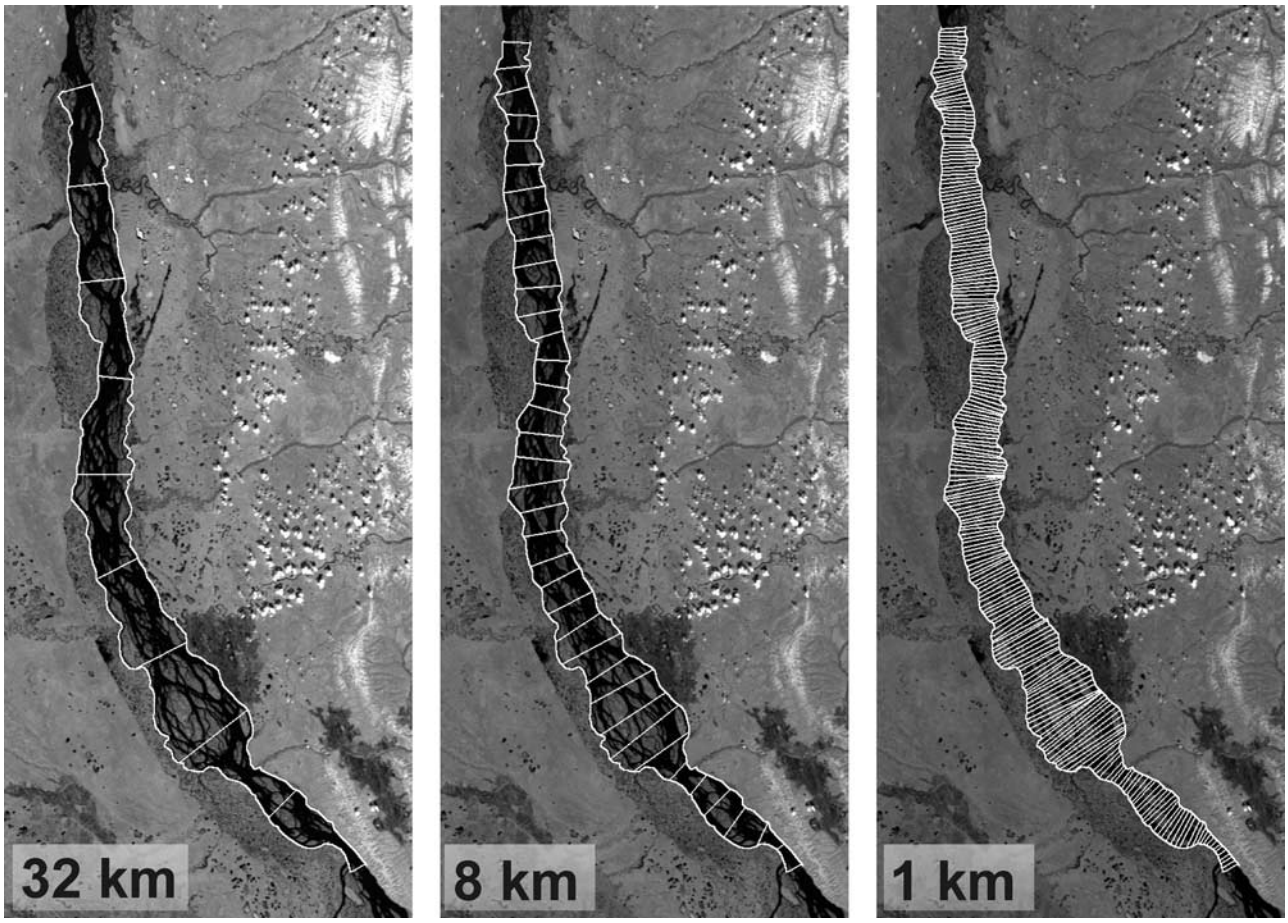

Figure 2. Sample MODIS image of the large braided reach used in this study, illustrating disaggregations of 32, 8, and 1 km reach length scales. Water surfaces appear dark, and white objects are clouds.

[16] Table 1 presents satellite-derived W_e values from the upstream study reach, satellite-derived predictions for downstream discharge at Kusur station 8 d later (Q_p), actual discharges observed at Kusur station 8 d later (Q_{t+8}), and the difference between the predicted and observed discharge values ($Q_p - Q_{t+8}$). The rating curve used to compute Q_p is $W_e = 11.91\ Q_p^{0.59}$ ($r^2 = 0.85$) constructed using the seventeen Kusur station Q measurements for 2001, the only year for which high-quality corrected discharge data are available. The rating curve fit through all Q data including provisional (not used) is $W_e = 38.7\ Q_p^{0.49}$ ($r^2 = 0.77$). Of necessity, all comparisons with subsequent years (2002–2005 Q, Table 1) must use provisional Kusur station data (http://rims.unh.edu/data.shtml).

[17] Agreement between satellite-predicted and Kusur station discharge is generally high (linear $r^2 = 0.94$ for 2001, 0.82 for 2002–2005, 0.81 across all years). Absolute differences between the two measurements ($Q_p - Q$, Table 1) are lowest in 2001, the calibrating year (mean = 11 ± 9%, median = 12%, range 1–29%). Absolute differences increase in 2002–2005, when no ground data were used for calibration (mean = 27 ± 22%, median = 20%, range 3–94%). Despite having the greatest passage of time since the calibrating year, absolute differences are lower in 2005 than either 2003 or 2004 (mean = 18 ± 9%, median = 18%, range 5–31%). Absolute differences across all years are 23 ± 20%, 17%, and 1–94% for mean, median and range, respectively. Note that the extent to which the generally larger 2002–2005 Q_p "errors" may be in fact be caused by the low quality of the provisional post-2001 gauging station data with which they are being compared cannot be assessed until corrected data are released by SHI.

[18] Intrinsic measurement error for ground-based discharge data at Kusur station has previously been estimated at ~6% for June–September [*Shiklomanov et al.*, 2006]. If river flows are assumed to be constant throughout the day (reasonable for a river this large), then small $W_e - Q_p$ contrasts between same-day MODIS images (nine dates, Table 1) can be attributed to intrinsic measurement error in our remote sensing methodology. This error is estimated as ±305 m (~5%) for W_e and ±325 m^3/s (~2%) for Q_p.

4.2. Scaling and Hydraulic Geometry

[19] The remotely sensed discharge retrievals presented in Table 1 are derived from a single W_e measurement for the entire study reach (316 km, Figure 3). In this section, we disaggregate the reach into a series of successively smaller subreaches, to explore how reach length scale impacts the transferability of resulting $W_e - Q$ rating curves from one location to another. The prime motivation for this is that morphology differences between sites, or changes over time at the same site, are thought to cause drifting of the

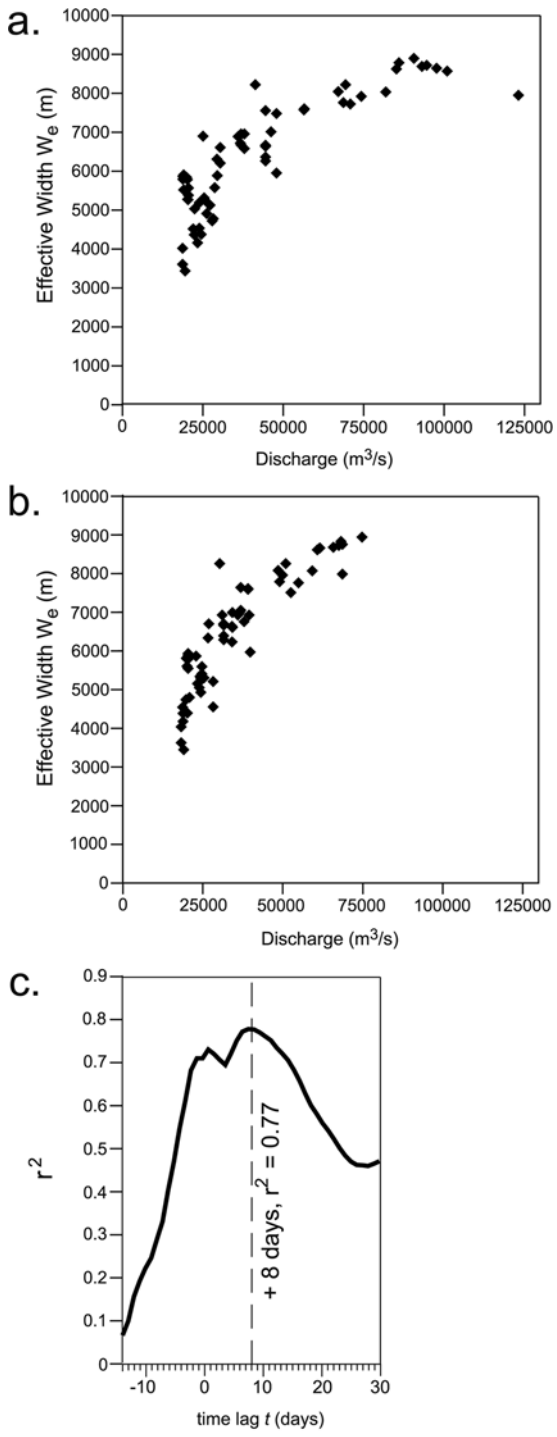

Figure 3. (a) A power law relationship is found between satellite-derived effective widths (W_e) and same-day ground measurements of river discharge (Q). (b) However, $W_e - Q$ rating curve scatter decreases when a time lag is introduced between the two variables. (c) Maximum correlation is achieved by lagging observed Q 8 d behind satellite-derived W_e, obtained ~700 km upstream.

relationship between W_e and Q [*Smith et al.*, 1996, 1997; *Ashmore and Sauks*, 2006], thereby precluding its use over time or to other locations. This problem leads *Ashmore and Sauks* [2006, p. 9] to conclude, "The length of river needed for spatial averaging to provide a stable width-discharge relationship requires more investigation," and is the purpose behind this section.

[20] For each of the 65 cloud-free MODIS images listed in Table 1, the study reach was successively disaggregated into a series of 1 to 1,264 successively finer subreaches, with length scales ranging from 256 to 0.25 km. $We - Q$ rating curves and *b* exponents were extracted for each. For illustration purposes, disaggregations of 32 km, 8 km, and 1 km length scales are shown in Figure 2, however 0.25–1 km increments were used to produce the fullest possible spectrum of length scales (note that this causes total river length analyzed to vary slightly and the number of subreaches to decrease at longer length scales). At the finest possible length scale (i.e., one MODIS pixel or 250 m) the segments collapse to a continuous series of 1,264 1-pixel-wide transects, analogous to a series of cross sections drawn every 250 m along the river course. Because there are no major tributaries or diversions within the study area and Lena River discharge is gradually varying, mean daily discharge was assumed constant throughout all subreaches to simplify computation of the $W_e - Q$ rating curves and *b* exponents. Note that this assumption introduces some error owing to the mean propagation speed of ~1 m s^{-1} (section 4.1). Also recall from section 2 that the obtained *b* exponents are based on reach-averaged widths rather than one-dimensional transects. As such, they most closely resemble classical *b* exponent measurement at the shortest length scales.

[21] The satellite-derived rating curves and *b* exponents clearly converge toward stable values as the subreach length scale is increased. Figure 4 illustrates this graphically, by plotting all $W_e - Q$ rating curves obtained for ten length scales ranging from 0.5 to 256 km. Note that these rating curves are computed identically as in Figure 2b, except far more of them are generated (one for each subreach). Visual inspection of the ten subreach length scales shown in Figure 4 suggests that the rating curves approach similarity by 128 km.

[22] The full spectrum of the disaggregation analysis can be seen by plotting all generated *b* exponents (equivalent to the slope of the $W_e - Q$ rating curve in log-log space) as a function of length scale (Figure 5). Visual inspection of Figure 5 suggests that the rating curve stabilization occurs by length scales of ~90 km. A more quantitative assessment is that at length scales ≥62 km all *b* exponents lie within ±10% of the overall reach average ($b = 0.48$). This translates to a maximum uncertainty of less than ±5% in discharge between different locations along the waterway.

[23] From both Figure 4 and Figure 5, it is clear that the satellite-derived $W_e - Q$ rating curves and *b* exponents display considerable variability at length scales below 32 km, and extreme variability (i.e., highest site specificity) at the shortest length scale (250 m). However, at length scales beyond ~60–90 km, approximately 2–3 times valley width, site specificity declines and the *b* exponents converge toward a characteristic value of $b = 0.48$. Put another way, at length scales exceeding ~60–90 km all subreaches display similar behavior everywhere. The precise length scale at which values of *b* stabilize depends on both the geometry of the river system and, potentially, on the resolution of the imagery used in the analysis. It is possible that area-

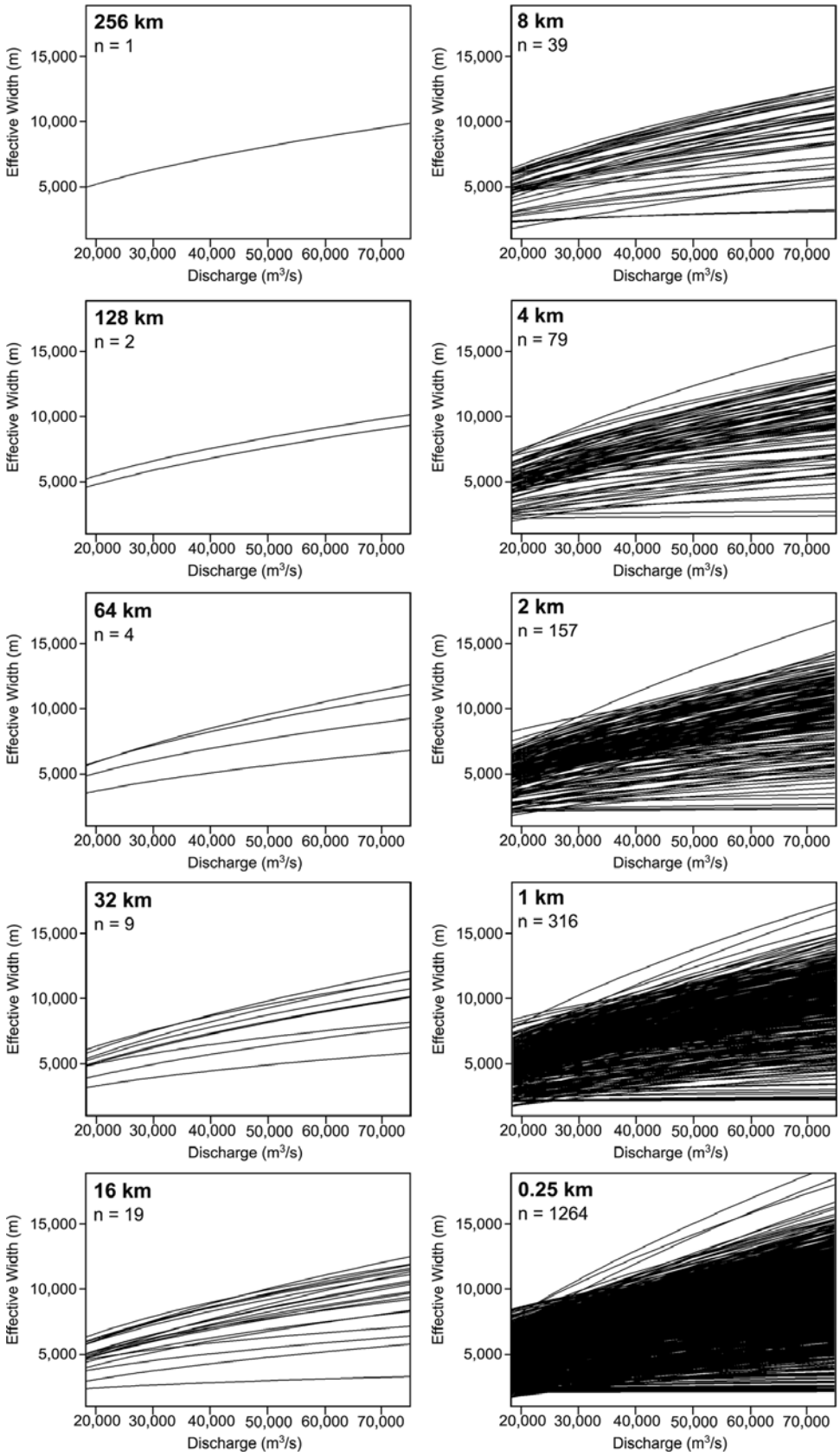

Figure 4. Distribution of best fit $W_e - Q$ rating curves for 10 example reach length scales. Each rating curve is obtained from a different location along the river. Rating curves from different river reaches display increasing similarity as reach length is increased.

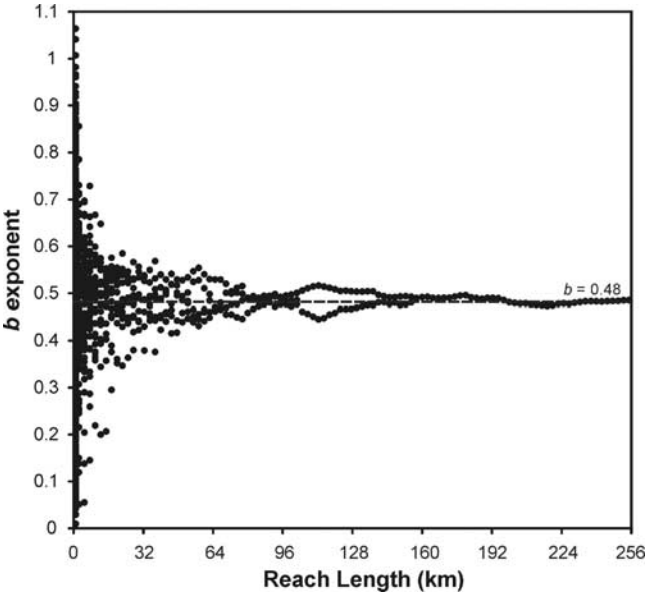

Figure 5. Distribution of *b* exponents for the full spectrum of reach length scales examined in this study (0.25–256 km). Convergence to a stable value (b = 0.48) is achieved at length scales > ~60–90 km (2–3 times floodplain valley width).

discharge relationships would become uniform at shorter length scales if imagery with higher spatial resolution were used.

[24] Figures 4 and 5 and calculations show that by measuring W_e with a sufficiently large length scale, spatial variability in the "sensitivity" of river width to discharge is reduced to single-digit uncertainty. This is an important result for the purpose of rating-curve transferability as described before. However, at finer spatial scales the remotely sensed *b* exponents display considerable variability, much like a series of field transects taken at different locations along a river channel. Indeed, it is exactly this high local-scale variability that imposes such site specificity (and need for empirical calibration) upon traditional, point-based discharge measurements. The local variations, however, are of value to fluvial geomorphologists and aquatic ecologists interested in hydraulic geometry, stream behavior, and habitat studies. Even for remote sensing applications, it is beneficial to identify tributary stream junctions, point bars, and other features that have high *b* exponents, i.e., are sensitive to small discharge variations [*Brakenridge et al.*, 2007]. Therefore, an additional advance of this study is the recovery of *b* exponents continuously along a river course (Figure 6). This represents, for the first time, the direct mapping of this classical hydraulic geometry parameter from space.

5. Discussion and Conclusion

[25] There are two new conclusions to be drawn from this analysis. The first is that remotely sensed effective width (W_e) variations are surprisingly well correlated (r^2 = 0.81) with ground measurements of river discharge taken days later hundreds of kilometers downstream. This broadens the prospective value of satellite-based discharge retrievals, i.e., from being a poor substitute for ground-based gauging stations to a predictive tool that can aid river forecasting. Satellite-based discharge retrievals will never achieve the precision of in situ streamflow measurements and should not, therefore, be aimed at "gauge replacement" strategies [*Alsdorf et al.*, 2007]. The real power of remote sensing instead lies in the ease with which it can be directed at remote river systems or provide a spatial view between existing point-based measurements. From a practical perspective, hydrologic monitoring agencies, reservoir operators, and watershed managers all stand to benefit from improved discharge forecasts that incorporate upstream remote sensing. Flow routing, a key task of all watershed hydrology models that estimates the timing and attenuation of a flood wave as it passes downstream, requires knowledge of flow propagation speed and is typically estimated using Muskingum-Cunge methods [*Ponce and Yevjevich*, 1978]. Results from this study demonstrate that mean channel flow propagation speeds may be estimable from space, simply by adjusting the time lag between upstream and downstream flow variations until maximum correlation is achieved. It seems plausible that spatial variations in propagation speed could be estimated in this way even in the total absence of ground data, simply by correlating W_e variations between many distributed locations posted along a river network. Such information, together with the magnitudes of the W_e changes themselves, might usefully be assimilated into watershed models to improve real-time forecasting of river discharge. In the present study we assumed a constant time lag (t = 8 d) but in practice the lag likely shortens with increasing discharge, perhaps explaining our apparent overestimation during high flows (Table 1). More work is needed to address this issue.

[26] The second key finding is that satellite-derived $W_e - Q$ rating curves and *b* exponents converge at length scales greater than ~60–90 km, roughly two to three times

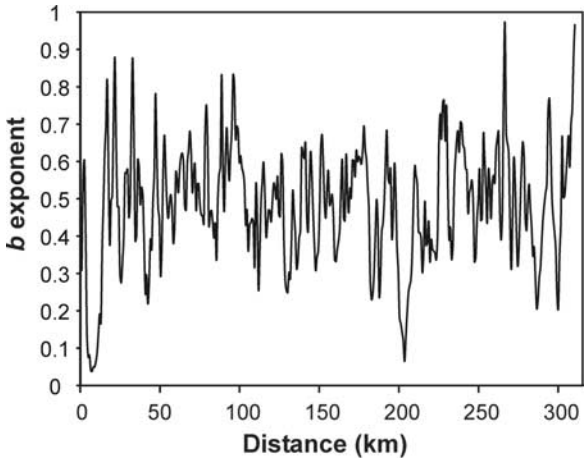

Figure 6. The first continuous mapping of a classical hydraulic geometry parameter from space. Longitudinal transect of MODIS-derived *b* exponents (1 km resolution, upstream is at left) revealing downstream variations in the sensitivity of flow width to discharge along the Lena River. The *b* exponent indicates the proportion of discharge that is accommodated by adjustments to flow width and is traditionally used in field-based fluvial studies as a diagnostic measure of river behavior and channel form.

the width of the Lena River floodplain. This has immediate practical importance for space-based discharge estimation techniques. As described earlier, the high site-specificity of both ground- and satellite-based rating curves is the prime obstacle to their application to other rivers or to different locations along the same river. Results from this study suggest that if a sufficiently large river reach length scale is defined, site-specificity declines and the derived rating curves become increasingly transferable to other locations along the waterway. This also revives hope for the possibility of a family of "universal" rating curves, associated with different river types, from which reasonable estimates of absolute discharge can be made even in ungauged rivers [*Smith et al.*, 1996; *Bjerklie et al.*, 2003]. However, the extent to which the transferability identified here holds true or breaks down across major transitions in river form (e.g., from braided to single channel) or between different rivers is a key question for future research. In the meantime, an immediate implication of this result concerns temporal sampling: Even with daily (or better) overpasses from two satellites, only 65 MODIS images and 53 of 610 target dates were completely cloud free over the 300 km study reach, less than 10% of the potential sampling rate. However, if a useful discharge estimate can be retrieved from any one of many candidate subreaches, then temporal sampling would be vastly improved by "cloud peeking," i.e., exploiting small openings in cloud cover to extract a useful W_e measurement from whatever subreach is visible along a river course. We estimate this refinement might potentially improve the temporal sampling to weekly or better for MODIS data over very large rivers.

[27] The finding of rating curve and *b* exponent convergence with increasing reach length also contributes to ongoing theoretical work on hydraulic geometry and spatial scaling in natural river systems. Following the seminal work of *Leopold and Maddock* [1953] most studies of hydraulic geometry were preoccupied with identifying similarities in *b*, *f*, and *m* among different rivers and attributing them to differences in climatic, geologic, or physiographic regime [*Park*, 1977]. This fell out of vogue as studies of large numbers of cross sections revealed the high degree of local complexity in natural channels, veering scientific interest toward the physical processes underlying those deviations [*Knighton*, 1974; *Richards*, 1976; *Phillips*, 1990]. Most recently, there has been renewed interest in identifying generalized hydraulic geometry relationships, through "reach averaging" of traditional cross sections [*Jowett*, 1998], multiscaling techniques [*Dodov and Foufoula-Georgiou*, 2004], and spatial studies of variability to obtain "reach hydraulic geometry relations" [*Stewardson*, 2005]. The present research provides independent verification that generalized hydraulic geometry relationships can indeed be identified through reach averaging, in this case using remote sensing. Furthermore, the convergence toward a characteristic *b* exponent at multiple length scales (Figure 5) lends support to previous assertions of self-similar scaling behavior in braided rivers [*Sapozhnikov and Foufoula-Georgiou*, 1996, 1997; *Nykanen et al.*, 1998; *Foufoula-Georgiou and Sapozhnikov*, 2001], and counters the notion that hydraulic geometry is unavoidably chaotic [*Phillips*, 1990].

[28] From a methodological standpoint, Figure 6 demonstrates for the first time that remote sensing can be used to map *b* exponents, a classical field-based parameter in hydraulic geometry, continuously along a river course. Currently, the vast majority of *b* exponent data are from river cross sections at permanent gauging stations, typically located in narrow, stable cross sections therefore biasing the sample pool [*Bjerklie et al.*, 2003]. And looking ahead, the limitations of hydraulic geometry may be laid bare by fully three-dimensional, spatially distributed studies of river behavior afforded by remote sensing [e.g., *Lane et al.*, 2003; *Carbonneau et al.*, 2006], perhaps moving us in an entirely new direction from the power law approach presented here.

[29] It is important to point out that the remotely sensed discharge retrievals and hydraulic geometry relationships reported here are made possible by the high correlation between "width" (inundation area) and discharge in braided rivers. Under bankfull flow conditions, an identical experiment for an entrenched, single-channel river is unlikely to generate the steep $W_e - Q$ rating curves and high *b* exponents seen here. Even for this heavily braided reach of the Lena River, the characteristic *b* exponent of 0.48 means that less than one half of the total variability in discharge is accommodated by W_e adjustments. Therefore, even for "width-sensitive" braided rivers like the Lena, a three-dimensional imaging technology that measures flow width, depth, and slope changes like the Surface Water Ocean Topography (SWOT) (see http://bprc.osu.edu/water/ and *Alsdorf et al.* [2007]) promises the most universal capability for space-based river studies.

[30] **Acknowledgments.** This research was funded by the NASA Terrestrial Hydrology Program grant NNG06GE05G. The MODIS satellite data were also provided by NASA. Crucial daily discharge data from Kusur station, and discussions on their quality were provided by A. I. Shiklomanov at the University of New Hampshire. The authors thank Robert Brakenridge, Timothy Martin, Greg Pasternack, and one anonymous reader for constructive reviews of this manuscript.

References

Al-Khudhairy, D. H. A., et al. (2002), Monitoring wetland ditch water levels using Landsat TM and ground-based measurements, *Photogramm. Eng. Remote Sens.*, *68*(8), 809–818.

Alsdorf, D. E. (2003), Water storage of the central Amazon floodplain measured with GIS and remote sensing imagery, *Ann. Assoc. Am. Geogr.*, *93*(1), 55–66.

Alsdorf, D. E., and D. P. Lettenmaier (2003), Tracking fresh water from space, *Science*, *301*, 1491–1494.

Alsdorf, D. E., J. M. Melack, T. Dunne, L. A. K. Mertes, L. L. Hess, and L. C. Smith (2000), Interferometric radar measurements of water level changes on the Amazon flood plain, *Nature*, *404*, 174–177.

Alsdorf, D., C. Birkett, T. Dunne, J. Melack, and L. Hess (2001), Water level changes in a large Amazon lake measured with spaceborne radar interferometry and altimetry, *Geophys. Res. Lett.*, *28*(14), 2671–2674.

Alsdorf, D. E., E. Rodríguez, and D. P. Lettenmaier (2007), Measuring surface water from space, *Rev. Geophys.*, *45*, RG2002, doi:10.1029/2006RG000197.

Andreadis, K. M., E. A. Clark, D. P. Lettenmaier, and D. E. Alsdorf (2007), Prospects for river discharge and depth estimation through assimilation of swath-altimetry into a raster-based hydrodynamics model, *Geophys. Res. Lett.*, *34*, L10403, doi:10.1029/2007GL029721.

Ashmore, P., and E. Sauks (2006), Prediction of discharge from water surface width in a braided river with implications for at-a-station hydraulic geometry, *Water Resour. Res.*, *42*, W03406, doi:10.1029/2005WR003993.

Bates, P. D., M. D. Wilson, M. S. Horritt, D. C. Mason, N. Holden, and A. Currie (2006), Reach scale floodplain inundation dynamics observed using airborne synthetic aperture radar imagery: Data analysis and modeling, *J. Hydrol.*, *328*, 306–318.

Birkett, C. M., L. A. K. Mertes, T. Dunne, M. H. Costa, and M. J. Jasinski (2002), Surface water dynamics in the Amazon Basin: Application of satellite radar altimetry, *J. Geophys. Res.*, *107*(D20), 8059, doi:10.1029/2001JD000609.

Bjerklie, D. M., S. L. Dingman, C. J. Vörösmarty, C. H. Bolster, and R. G. Congalton (2003), Evaluating the potential for measuring river discharge from space, *J. Hydrol.*, *278*, 17–38.

Bjerklie, D. M., D. Moller, L. C. Smith, and S. L. Dingman (2005), Estimating discharge in rivers using remotely sensed hydraulic information, *J. Hydrol.*, *309*, 191–209.

Brakenridge, G. R., J. C. Knox, E. D. Paylor, and F. J. Magilligan (1994), Radar remote sensing aids study of the great flood of 1993, *Eos Trans. AGU*, *75*(45), 521.

Brakenridge, G. R., B. T. Tracy, and J. C. Knox (1998), Orbital SAR remote sensing of a river flood wave, *Int. J. Remote Sens.*, *19*(7), 1439–1445.

Brakenridge, G. R., S. V. Nghiem, E. Anderson, and S. Chien (2005), Space-based measurement of river runoff, *Eos Trans. AGU*, *86*(19), 185.

Brakenridge, G. R., S. V. Nghiem, E. Anderson, and R. Mic (2007), Orbital microwave measurement of river discharge and ice status, *Water Resour. Res.*, *43*, W04405, doi:10.1029/2006WR005238.

Calmant, S., and F. Seyler (2006), Continental surface waters from satellite altimetry, *C. R. Geosci.*, *338*, 1113–1122.

Carbonneau, P. E., S. N. Lane, and N. Bergeron (2006), Feature based image processing methods applied to bathymetric measurements from airborne remote sensing in fluvial environments, *Earth Surf. Processes Landforms*, *31*, 1413–1423.

Chalov, R. S. (2001), Intricately braided river channels of lowland rivers: Formation conditions, morphology, and definition, *Vodnye Resursy*, *28*(2), 166–171. (*Water Resour.*, Engl. Transl., *28*(2), 145–150.)

Coe, M. T., and C. M. Birkett (2004), Calculation of river discharge and prediction of lake height from satellite radar altimetry: Example for the Lake Chad basin, *Water Resour. Res.*, *40*, W10205, doi:10.1029/2003WR002543.

Dodov, B., and E. Foufoula-Georgiou (2004), Generalized hydraulic geometry: Derivation based on a multiscaling formalism, *Water Resour. Res.*, *40*, W06302, doi:10.1029/2003WR002082.

Ferguson, R., and P. Ashworth (1991), Slope-induced changes in channel character along a gravel-bed stream: The Allt Dubhaig, Scotland, *Earth Surf. Processes Landforms*, *16*, 65–82.

Foufoula-Georgiou, E., and V. Sapozhnikov (2001), Scale invariances in the morphology and evolution of braided rivers, *Math. Geol.*, *33*(3), 273–291.

Frappart, F., F. Seyler, J. M. Martinez, J. G. Leon, and A. Cazenave (2005), Floodplain water storage in the Negro River basin estimated from microwave remote sensing of inundation area and water levels, *Remote Sens. Environ.*, *99*(4), 387–399.

Frappart, F., K. Do Minh, J. L'Hermitte, A. Cazenave, G. Ramillien, T. Le Toan, and N. Mognard-Campbell (2006), Water volume change in the lower Mekong from satellite altimetry and imagery data, *Geophys. J. Int.*, *167*(2), 570–584.

Grippa, M., N. M. Mognard, T. Le Toan, and S. Biancamaria (2007), Observations of changes in surface water over the western Siberia lowland, *Geophys. Res. Lett.*, *34*, L15403, doi:10.1029/2007GL030165.

Horritt, M. S., and P. D. Bates (2002), Evaluation of 1D and 2D numerical models for predicting river flood inundation, *J. Hydrol.*, *268*, 87–99.

Hudson, P. F., and R. R. Colditz (2003), Flood delineation in a large and complex alluvial valley, lower Pánuco basin, Mexico, *J. Hydrol.*, *280*, 229–245.

Jowett, I. G. (1998), Hydraulic geometry of New Zealand rivers and its use as a preliminary method of habitat assessment, *Reg. Rivers Res. Manage.*, *14*, 451–466.

Knighton, A. D. (1974), Variation in width-discharge relation and some implications for hydraulic geometry, *Geol. Soc. Am. Bull.*, *85*, 1069–1076.

Kouraev, A. V., E. A. Zakharova, O. Samain, N. M. Mognard, and A. Cazenave (2004), Ob' river discharge from TOPEX/Poseidon satellite altimetry (1992–2002), *Remote Sens. Environ.*, *93*, 238–245.

Lane, S. N., R. M. Westaway, and D. M. Hicks (2003), Estimation of erosion and deposition volumes in a large, gravel-bed, braided river using synoptic remote sensing, *Earth Surf. Processes Landforms*, *28*, 249–271.

LeFavour, G., and D. Alsdorf (2005), Water slope and discharge in the Amazon River estimated using the shuttle radar topography mission digital elevation model, *Geophys. Res. Lett.*, *32*, L17404, doi:10.1029/2005GL023836.

Leon, J. G., S. Calmant, F. Seyler, M.-P. Bonnet, M. Cauhopé, F. Frappart, N. Filizola, and P. Fraizy (2006), Rating curves and estimation of average water depth at the upper Negro River based on satellite altimeter data and modeled discharges, *J. Hydrol.*, *328*, 481–496.

Leopold, L. B., and T. Maddock (1953), The hydraulic geometry of stream channels and some physiographic implications, *U.S. Geol. Surv. Prof. Pap.*, *252*, 57 pp.

Matgen, P., G. Schumann, J.-B. Henry, L. Hoffmann, and L. Pfister (2007), Integration of SAR-derived river inundation areas, high-precision topographic data and a river flow model toward near real-time flood management, *Int. J. Appl. Earth Obs. Geoinf.*, *9*(3), 247–263.

Nykanen, D. K., E. Foufoula-Georgiou, and V. B. Sapozhnikov (1998), Study of spatial scaling in braided river patterns using synthetic aperture radar imagery, *Water Resour. Res.*, *34*, 1795–1807.

Overton, I. C. (2005), Modelling floodplain inundation on a regulated river: Integrating GIS, remote sensing and hydrological models, *River Res. Appl.*, *21*, 991–1001.

Papa, F., C. Prigent, and W. B. Rossow (2007), Ob' River flood inundations from satellite observations: A relationship with winter snow parameters and river runoff, *J. Geophys. Res.*, *112*, D18103, doi:10.1029/2007JD008451.

Park, C. C. (1977), World-wide variation in hydraulic geometry exponents of stream channel: An analysis and some observations, *J. Hydrol.*, *33*, 133–146.

Pavelsky, T. M., and L. C. Smith (2004), Spatial and temporal patterns in Arctic river ice breakup observed with MODIS and AVHRR time series, *Remote Sens. Environ.*, *93*, 328–338.

Pavelsky, T. M., and L. C. Smith (2008), RivWidth: A software tool for the calculation of river width from remotely sensed imagery, *IEEE Geosci. Remote Sens. Lett.*, *5*(1), 70–73.

Phillips, J. D. (1990), The instability of hydraulic geometry, *Water Resour. Res.*, *26*, 739–744.

Ponce, V. M., and V. Yevjevich (1978), Muskingum-Cunge method with variable parameters, *J. Hydraul. Div. Am. Soc. Civ. Eng.*, *104*(12), 1663–1667.

Richards, K. S. (1976), Complex width-discharge relations in natural river sections, *Bull. Geol. Soc. Am.*, *87*, 199–206.

Richey, J. E., J. M. Melack, A. K. Aufdenkampe, V. M. Ballester, and L. L. Hess (2002), Outgassing from Amazonian rivers and wetlands as a large tropical source of atmospheric CO_2, *Nature*, *416*, 617–620.

Roux, H., and D. Dartus (2006), Use of parameter optimization to estimate a flood wave: Potential applications to remote sensing of rivers, *J. Hydrol.*, *328*, 258–266.

Sanyal, J., and X. X. Lu (2004), Application of remote sensing in flood managements with special reference to monsoon Asia: A review, *Nat. Hazards*, *33*, 283–301.

Sapozhnikov, V. B., and E. Foufoula-Georgiou (1996), Self-affinity in braided rivers, *Water Resour. Res.*, *32*, 1429–1439.

Sapozhnikov, V. B., and E. Foufoula-Georgiou (1997), Experimental evidence of dynamic scaling and indications of self-organized criticality in braided rivers, *Water Resour. Res.*, *33*, 1983–1991.

Schumann, G., R. Hostache, C. Puech, L. Hoffmann, P. Matgen, F. Pappenberger, and L. Pfister (2007), High-resolution 3-D flood information from radar imagery for flood hazard management, *IEEE Trans. Geosci. Remote Sens.*, *45*(6), 1715–1725.

Shiklomanov, A. I., R. B. Lammers, and C. Vörösmarty (2002), Widespread decline in hydrologic monitoring threatens Pan-Arctic research, *Eos Trans. AGU*, *83*(2), 13.

Shiklomanov, A. I., T. I. Yakovleva, R. B. Lammers, I. P. Karasev, C. J. Vörösmarty, and E. Linder (2006), Cold region river discharge uncertainty—Estimates from large Russian rivers, *J. Hydrol.*, *326*, 231–256.

Smith, L. C. (1997), Satellite remote sensing of river inundation area, stage, and discharge: A review, *Hydrol. Processes*, *11*, 1427–1439.

Smith, L. C. (2002), Emerging applications of interferometric synthetic aperture radar (InSAR) in geomorphology and hydrology, *Ann. Assoc. Am. Geogr.*, *92*(3), 385–398.

Smith, L. C., and D. E. Alsdorf (1998), Control on sediment and organic carbon delivery to the Arctic Ocean revealed with spaceborne synthetic aperture radar: Ob' River, Siberia, *Geology*, *26*(5), 395–398.

Smith, L. C., B. L. Isacks, R. R. Forster, A. L. Bloom, and I. Preuss (1995), Estimation of discharge from braided glacial rivers using ERS-1 synthetic aperture: First results, *Water Resour. Res.*, *31*, 1325–1329.

Smith, L. C., B. L. Isacks, A. L. Bloom, and A. B. Murray (1996), Estimation of discharge from three braided rivers using synthetic aperture radar satellite imagery: Potential application to ungaged basins, *Water Resour. Res.*, *32*, 2021–2034.

Smith, L. C., Y. Sheng, G. M. MacDonald, and L. D. Hinzman (2005), Disappearing Arctic lakes, *Science*, *308*, 1429–1429.

Stewardson, M. (2005), Hydraulic geometry of stream reaches, *J. Hydrol.*, *306*, 97–111.

Stocker, T. F., and C. C. Raible (2005), Water cycle shifts gear, *Nature*, *434*, 830–833.

Temimi, M., R. Leconte, F. Brissette, and N. Chaouch (2005), Flood monitoring over the Mackenzie River Basin using passive microwave data, *Remote Sens. Environ.*, *98*, 344–355.

Townsend, P. A., and J. R. Foster (2002), A synthetic aperture radar–based model to assess historical changes in lowland floodplain hydroperiod, *Water Resour. Res.*, *38*(7), 1115, doi:10.1029/2001WR001046.

Usachev, V. F. (1983), Evaluation of flood plain inundations by remote sensing methods, Proceedings of the Hamburg Symposium, *IAHS Publ.*, *145*, 475–482.

Vörösmarty, C. J., P. Green, J. Salisbury, and R. B. Lammers (2000), Global water resources: Vulnerability from climate change and population growth, *Science*, *289*, 284–288.

Wu, P., R. Wood, and P. Stott (2005), Human influence on increasing Arctic river discharges, *Geophys. Res. Lett.*, *32*, L02703, doi:10.1029/2004GL021570.

Xu, K., J. Zhang, M. Watanabe, and C. Sun (2004), Estimating river discharge from very high-resolution satellite data: A case study in the Yangtze River, China, *Hydrol. Processes*, *18*, 1927–1939.

Zhang, J. Q., K. Q. Xu, M. Watanabe, Y. H. Yang, and X. W. Chen (2004), Estimation of river discharge from non-trapezoidal open channel using QuickBird-2 satellite imagery, *Hydrol. Sci. J.*, *49*(2), 247–260.

T. M. Pavelsky and L. C. Smith, Department of Geography, University of California, 1255 Bunche Hall, Box 951524, Los Angeles, CA 90095-1524, USA. (lsmith@geog.ucla.edu)